WILEY-VCH

Doubly coated, organic – inorganic paraffin phase change materials: zinc oxide coating of hermetically encapsulated paraffins

Alexey A. Mikhaylov, Alexander G. Medvedev, Dmitry A. Grishanov, Sergey Sladkevich, Zhichuan J. Xu, Konstantin A. Sakharov, Petr V. Prikhodchenko, Ovadia Lev**

Dr. A. A. Mikhaylov, Dr. A. G. Medvedev, Dr. D. A. Grishanov, Dr. P. V. Prikhodchenko
Kurnakov Institute of General and Inorganic Chemistry, Russian Academy of Sciences, Leninskii prosp. 31, Moscow 119991, Russia.
E-mail: prikhman@gmail.com

Dr. A. A. Mikhaylov, Dr. A. G. Medvedev, Dr. S. Sladkevich, Dr. K. A. Saharov, Prof. O. Lev
The Casali Center of Applied Chemistry, The Institute of Chemistry The Hebrew University of Jerusalem Edmond J. Safra Campus, Jerusalem 91904, Israel.
E-mail: ovadia@mail.huji.ac.il

Dr. A. A. Mikhaylov, Dr. A. G. Medvedev, Dr. K. A. Saharov, Prof. Z. J. Xu, Prof. O. Lev
Singapore-HUJ Alliance for Research and Enterprise, NEW-CREATE Phase II Campus for Research Excellence and Technological Enterprise (CREATE) 1 CREATE Way, Singapore 138602, Singapore.

Prof. Z. J. Xu, Prof. O. Lev
School of Materials Science and Engineering, Nanyang Technological University 50 Nanyang Avenue, Singapore 639798, Singapore.

Keywords: phase change materials, zinc oxide, thermal conductivity

A way to benefit from the favorable attributes of both organic microencapsulation, including the hermetic sealing of the organic PCM core, and inorganic microencapsulation, including dispersibility in aqueous and polar solvents and improved thermal conductivity, is outlined. The approach is demonstrated by uniformly coating organic polymer encapsulated PCMs with zinc oxide, which allows thermal percolation through the interconnected inorganic shells. We demonstrate that hydrogen peroxide sol-gel processing can be used to form such uniform zinc peroxide coatings which are then converted by chemical treatment to zinc oxide shells. The way to overcome different challenges associated with the synthesis of thin film coatings of organic PCMs by zinc oxide are addressed, and the favorable attributes of the new doubly coated PCM capsules are demonstrated.

1. Introduction

Phase change materials, PCMs allow conversion of sensible heat to latent heat. Most useful energy storage PCMs involve organic compounds, and particularly paraffins and fatty acids. Paraffins, and organic PCMs in general, are less corrosive and have lower freeze-thaw hysteresis compared to inorganic ones. However, paraffins are flammable and have lower thermal conductivity (around 0.2 $J K^{-1} g^{-1}$) compared to metal hydrates and eutectic inorganic PCMs. [1–6] After melting, organic PCMs tend to coalesce, and form thick thermal insulating layers or large particles that are incompatible with flow systems. In addition, biocides, fire retardants and other additives tend to segregate out upon thermal cycling. One remedy to these drawbacks is microencapsulation to prevent segregation and coalescence. Organic and inorganic shells are used for microencapsulation of paraffins and other organic PCMs. The inorganic capsules, mostly silica and titania or graphene oxide and metallic silver decorations provide improved thermal conductivity, fire retardation and compatibility with inorganic building ingredients and flow systems.[7–13] However, it is practically impossible to maintain hermetic encapsulation of the small organic molecule melts within inorganic shells and retain zero leakage after many hundreds of freeze-thaw cycles, particularly when the weight fraction of the shell is to be kept low. Organic microcapsules offer better flexibility, and they also prevent leakage better, but they have lower thermal conductivity, lower flame retardation and lower compatibility with polar fluids and with inorganic building materials. A third way, proposed in this article, is to merge the two approaches: uniform coating of the paraffin core by organic polymer and external coating of the latter by an inorganic thin film as to maximize heat transfer and to endow the PCMs with the favorable properties of inorganic materials.

In this article, we introduce the synthesis of a zinc oxide coating onto organically encapsulated paraffin PCM substrates based on hydrogen peroxide sol-gel processing. A somewhat related approach involves the decoration of organic PCM capsules with silver metal spots and graphene oxide, though both alternatives rely on expensive additives. [12,14] We show that the coating process can be conducted at low temperature, which does not

damage the capsule or evaporate the organic core. Coating of capsules of paraffins by metal and metalloid oxides is not an easy task. Whereas the low temperature, thin film coating of large flat surfaces by spray-, dip-, spin-, and spread-coating and related thin film processing is relatively straightforward nowadays, the coating of particulates is, by and large, dominated by (hydro- and solvo-) thermal treatments and variants of the Pechini process which are both incompatible with thin film formation on microencapsulated paraffinic cores.[15–18] We stipulated that hydrogen peroxide sol-gel processing is an alternative coating pathway that should be explored, though, as outlined below, its application to coating of microencapsulated materials was less straightforward than anticipated. Hydroperoxo ligands stabilize d-10 and p-block element oxide and peroxide nanoparticles in aqueous solution (at moderate pH), and the resulting sol can be deposited on microparticulates by mild destabilization (vide infra).[19–23]

2. Results and discussion

As a substrate for the coating process, we chose the poly(melamine-formaldehyde) encapsulated, paraffin core PCMs, that are described in numerous publications, and are also commercially available from Microtek Laboratories Inc.[24–26] The native PCM microcapsules have spherical shape of uniform diameter of *ca.* 14-24 μM. They are very stable, their paraffin content does not leak out even after hundreds of freeze-thaw cycles, and the thickness of their shell is impressively thin, resulting in a specific latent heat of > 150 $J\,K^{-1}\,cm^{-1}$. Microtek Laboratories Inc. offers a range of paraffin PCMs, and we have chosen to demonstrate the zinc oxide coating on two brands, MCT28 and MCT68 which undergo phase change around 28 °C and 68 °C, i.e. close to the human comfort level and in the useful range of domestic solar heaters, respectively.

Zinc oxide was chosen as the external shell material due to its transparency,[27] biocidal activity, lack of toxicity and favorable flame retardation properties. [28–30] Encapsulation of paraffin PCMs in biocidal zinc oxide was recently reported.[31] Our first attempts to coat the

PCM microbeads were directed towards straightforward, mild thermal treatments with zinc salts under slightly basic pH. However, since these were unsuccessful, we heated the aqueous dispersion of beads (without zinc) at 130 °C for 3 hrs. Even under these mild conditions, the beads were deformed as can be seen in **Figure 1**b (compared to the native encapsulated PCMs in Figure 1a), which explained the failure of the hydrothermal synthesis. We also tried to coat the capsules by immersion in acidic zinc acetate solution and increasing the pH gradually by adding ammonia to induce precipitation, hoping for preferable precipitation on the capsules. However, homogeneous nucleation and growth of zinc hydroxide was predominant, and nonspecific deposition outside the microcapsules took place (Figure 1c). For similar thermal stability reasons, the Pechini route was not attempted, though zinc oxide formation by the Pechini route has been reported.[18] Therefore, we reverted to the hydrogen peroxide sol-gel process involving the deposition of zinc peroxide as a first stage.Deposition of thin zinc peroxide films on mica by a hydrogen peroxide sol-gel process has already been reported.[32] In this work, the coating procedure was modified to obtain a zinc peroxide coating on PCM capsules.

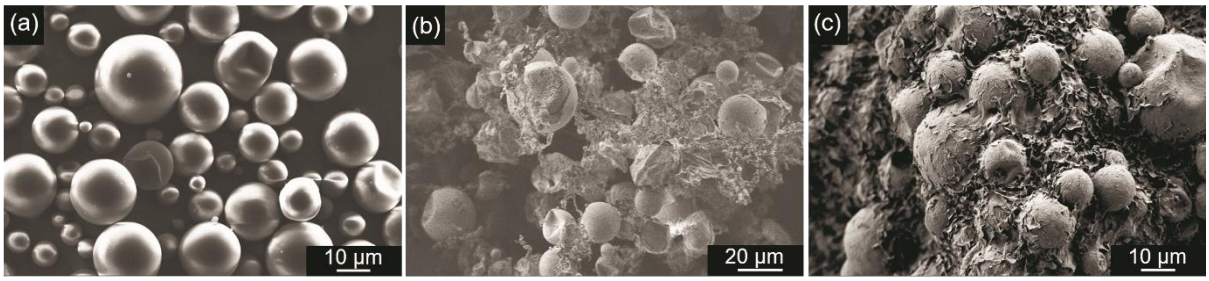

Figure 1. Bare MCT28 (a), MCT28 beads after heat treatment at 130 °C for 3 hrs in an autoclave (b). A failed attempt to deposit zinc oxide on PCMs by raising the pH of MCT28 dispersed in zinc acetate (c).

The deposition is based on the formation of zinc peroxide sol and then hydrogen bonding of surface peroxogroups to hydrogen acceptors on the (PCM) substrate. Hydrogen peroxide is a better hydrogen donor than water, and therefore, the bonding of the hydroperoxo groups, which are abundant on the zinc peroxide particles is preferred over water.[33] Terminal ZnOOH moieties can readily form hydrogen bonds to the triazine nitrogen and to the methylol

oxygen acceptors on the melamine-formaldehyde copolymer. Scraborough's team has recently shown that Zn - coordinated hydrogen peroxide forms strong hydrogen bonds as a hydrogen donor with oxygen atoms of organic ligands, a system that closely resembles the attachment of zinc hydroperoxo terminal groups to the nitrogen and oxygen containing surface of melamine-formaldehyde copolymer.[34] In our process, zinc acetate was added to a solution containing ammonia and a dispersion of PCM substrate, and subsequently hydrogen peroxide was added slowly to the stirred dispersion. Hydrogen peroxide addition served two complementing tasks, it lowered the pH and cleaved the ammonia – zinc complexes and thus formed zinc peroxide nanoparticles, in accordance with ref., and those were immediately deposited on the solid surface.[32] **Figures 2** (a-c) demonstrate the morphology of the encapsulated PCMs after zinc peroxide deposition. The micrograph shows that the capsules were coated by a uniform and complete layer of zinc peroxide, rather than mere decoration by zinc peroxide aggregates. Similar results were obtained for MCT68 (Figure 2 d-f).

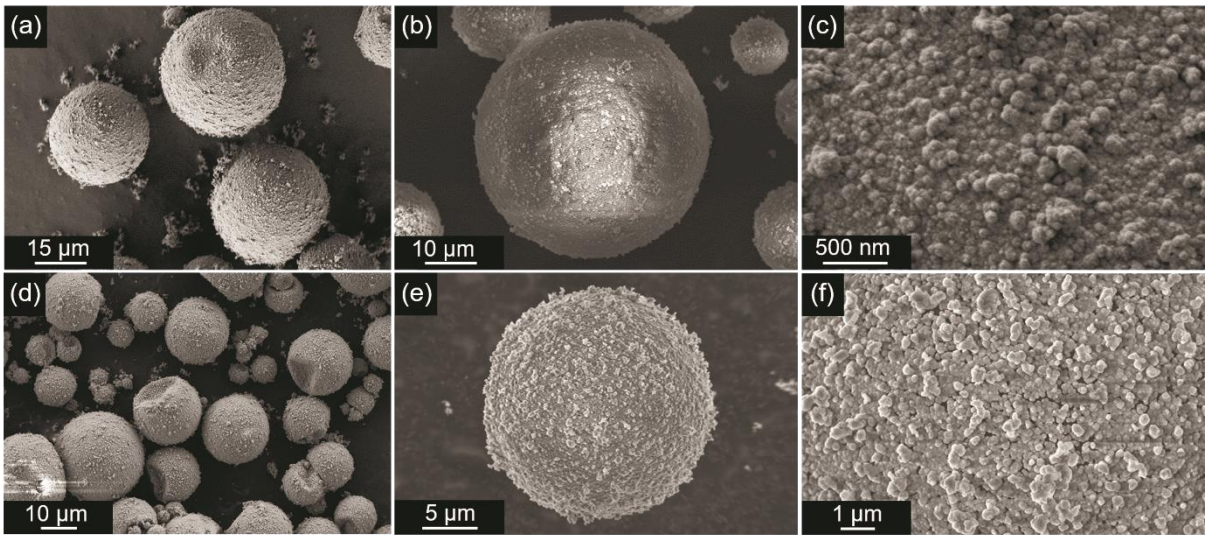

Figure 2. SEM images of MCT28-ZnO (a)-c)), MCT68-ZnO (d)-f)), at different magnifications.

The crystalline nature of the cubic zinc peroxide (PDF 00-013-0311) is apparent in diffractograms presented in **Figure 3**. The crystalline phase could be indexed to the cubic ZnO_2 with a=4.871 A (space group Pa-3) and the crystallite size is 28.8 nm as determined by

Scherrer equation. The characteristic peaks of n-octadecane are also apparent in the range 2θ = 20-25. We performed Rietveld refinement of powder XRD data using the crystalline phases of n-octadecane and cubic ZnO_2. The amorphous background described by a single broad peak is presented in Figure S1 of the ESI. The degree of crystallinity is 81%, but the amorphous peak position indicates that the amorphous part is largely contributed by the organic phase. Figure S1 shows that the error after subtraction of the single peak amorphous signal and the crystalline phases is indeed random and insignificant.

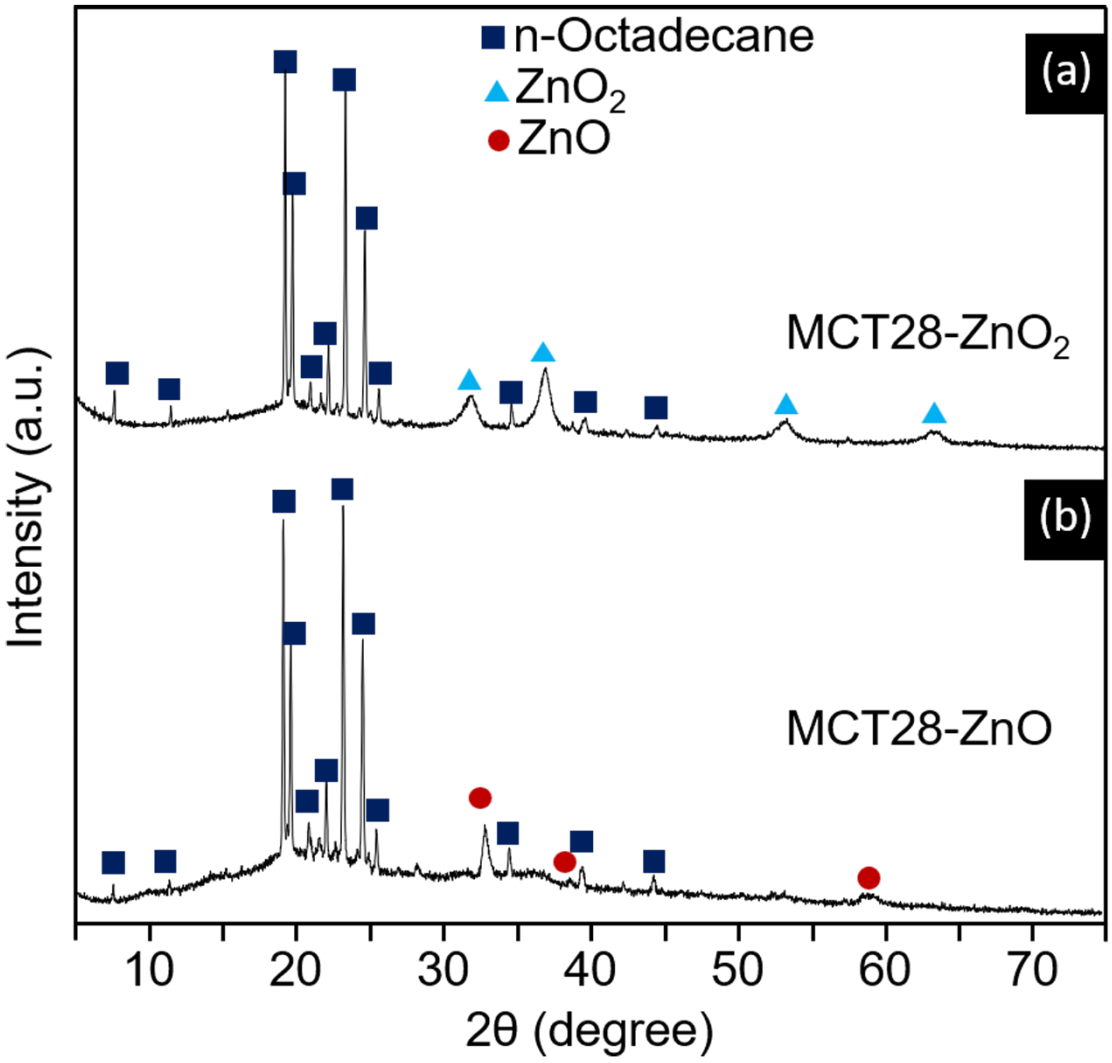

Figure 3. Powder X-ray diffractograms of zinc peroxide coated MCT28 a) and MCT28-ZnO-2 b). Library patterns of hexagonal zincite ZnO (PDF 01-071-6424), cubic ZnO_2 (PDF 00-013-0311), and n-octadecane are also shown.

Although, in principle, zinc peroxide is a stable material and can be left in the end-product, we anticipated that it would eventually deteriorate over a long exposure to the harsh environmental conditions, and despite its thermal stability the availability of peroxide in the vicinity of organics should not be encouraged for safety reasons. We therefore attempted to remove the peroxide by thermal treatment. Since the DSC of zinc peroxide showed that it begins to deteriorate at 180 °C we conducted the thermal peroxide decomposition treatments at 150°C for prolonged duration.[32] After 4 *hrs* the beads were distorted (see Figure S2), but still some peroxide remained intact as determined qualitatively by permanganometric titration. We tried to treat the capsules with $NaBH_4$ for 1h at 70 °C, which resulted in zinc oxide peel off. The zinc peroxide coated and uncoated MCT28 (Figure S2) suffered similar damage after heat treatment (as shown in figure S2).

Therefore, we tried several chemical (Figure S3), and tried heat treatment at 100 °C in H_2 atmosphere, which did not affect the X-ray diffractogram. Finally, the most successful approach involved sodium sulfite reduction in aqueous dispersion. Complete conversion of the peroxide to the respective oxide was observed after 3 days at room temperature. We did not attempt to optimize the temperature, sulfite concentration and the reaction time.

Figure 3 confirmed the absence of the cubic zinc peroxide phase and the formation of hexagonal zincite phase with a = 3,2494 Å , c = 5.2038 Å (space group P63mc) crystal parameters (PDF 01-071-6424), and 12.9 nm crystallite size. Rietveld refinement of the powder XRD data using crystalline phases of the n-octadecane and the hexagonal zinc oxide and a description of the amorphous phase by a single peak (at 20.1 degrees) allowed us to estimate that the degree of crystallinity is approximately 77% (Figure S1). However, again, most of the amorphous phase is attributed to the paraffin core and its organic capsule and not to the zinc peroxide phase.

We examined the possibility of changing the zinc oxide loading by altering the zinc concentration in the starting solution. The morphologies of the zinc peroxide coatings at

different zinc loadings are demonstrated in **Figure 4**. Using a weight ratio of 13:1 between the PCM and zinc acetate gave the optimal results (Figure 4 b)-e)). Using a twice larger concentration of zinc acetate (corresponding to a ratio of 6.5:1) resulted in a somewhat rougher surface, whereas decreasing the ratio by 33% (i.e., 19.7:1) resulted in incomplete coating of the microcapsules by zinc oxide and bare islands of melamine-formaldehyde copolymer remained on the surface. (Figure 4 c,f).

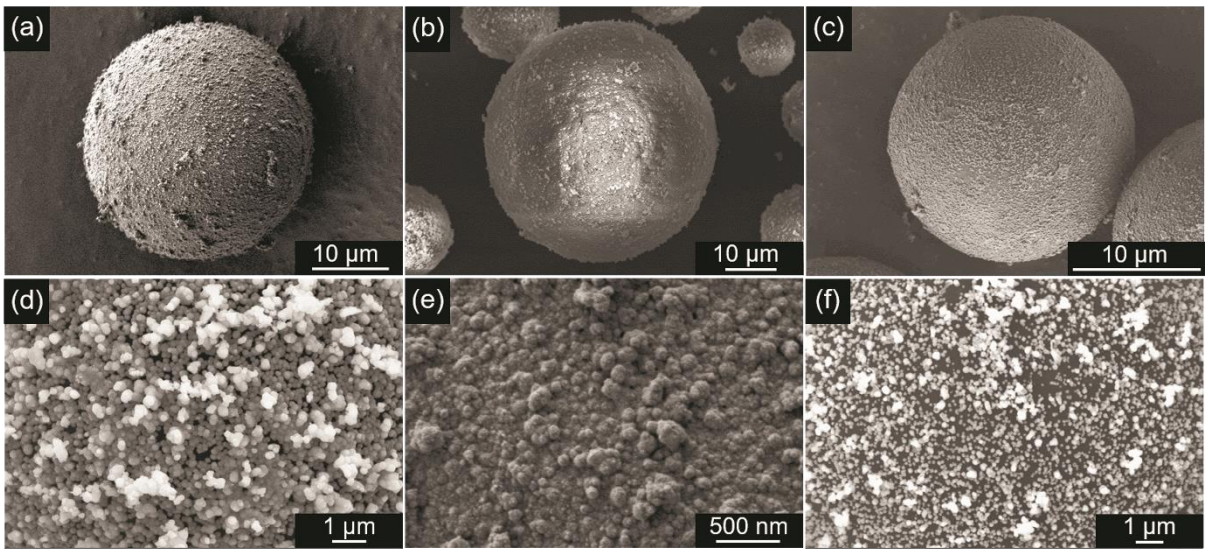

Figure 4. SEM images of MCT28-ZnO-1 (a, d)), MCT28-ZnO-2 (b, e)), MCT28-ZnO-3 (c, f)) at different magnifications.

The elemental analysis of the three films as compared to the bare PCM capsules is depicted in Table 1. EDAX of the coated film confirmed the presence of the zinc oxide film on the surface. The table indicates that, indeed, the amount of zinc acetate in the solution is a viable way to control zinc oxide loading on the PCM. The higher the zinc acetate the larger the zinc oxide loading. However, this way to quantify the Zn loading can be used to obtain a qualitative trend only, because the EDAX contribution of the melamine - formaldehyde copolymer and the paraffin core are underestimated due to shielding by the outer zinc oxide coating. A better way to measure the zinc oxide loading is by calorimetric analysis (DSC), which allows more accurate determination of the encapsulated paraffin (vide infra).

Table 1. Elemental analysis of MCT28-ZnO-1, MCT28-ZnO-2, MCT28-ZnO-3

Sample	C (wt/at)	N (wt/at)	O (wt/at)	Zn (wt/at)	ZnAcet (as Zn) :PCM (wt ratio)	Paraffin percentage estimated by DSC[a)]	Zinc oxide percentage estimated by TG[b)]
MCT28-ZnO-1	62.4/69.9	22.1/21.2	9.0/7.5	6.4/1.3	1:6.5	50.4	12
MCT28-ZnO-2	64.0/68.7	28.5/26.2	5.83/4.7	1.8/0.4	1:13	55.9	9
MCT28-ZnO-3	69.2/73.2	26.4/23.4	3.3/2.6	1.1/0.2	1:19.7	61.3	5
Uncoated MCT28	72.0/76.34	21.2/19.0	5.89/4.62	-	-	65.0	-

[a)] assuming heat of fusion of the paraffin core = 256 J g^{-1}; [b)] Zinc oxide content was quantified by the weight fraction of the residual inorganic phase after combustion of the organic material and assuming negligible water loss due to condensation reactions and complete elimination of the nitrogen containing compounds by the heat treatment

The structure of the inorganic coating was examined also by heat treatment at elevated temperature (900 °C) in air. The micrographs (Figure S4) demonstrate the morphology of the inorganic capsule alone after heat treatment. Clearly, MCT-ZnO-2 exhibited the most uniform and smoothest morphology of the coating. The capsule kept its spherical shape, though it is disrupted by small holes that are presumably formed by the release of the combustion gases. In order to study the morphology of the double coatings we carried out galium Focused Ion Beam (FIB) analysis of a PCM microsphere. FIB etching of MCT28-ZnO-2 gave an empty half sphere of *ca* 20 microns. The inner paraffinic core evaporated during the process (**Figure 5**). A zoom-in micrograph of the double core, shown in frame b), reveals two layers, the melamine – formaldehyde capsule, of approximately 300 nm and an outer zinc oxide layer, which is considerably rougher, and its thickness is approximately 400 nm.

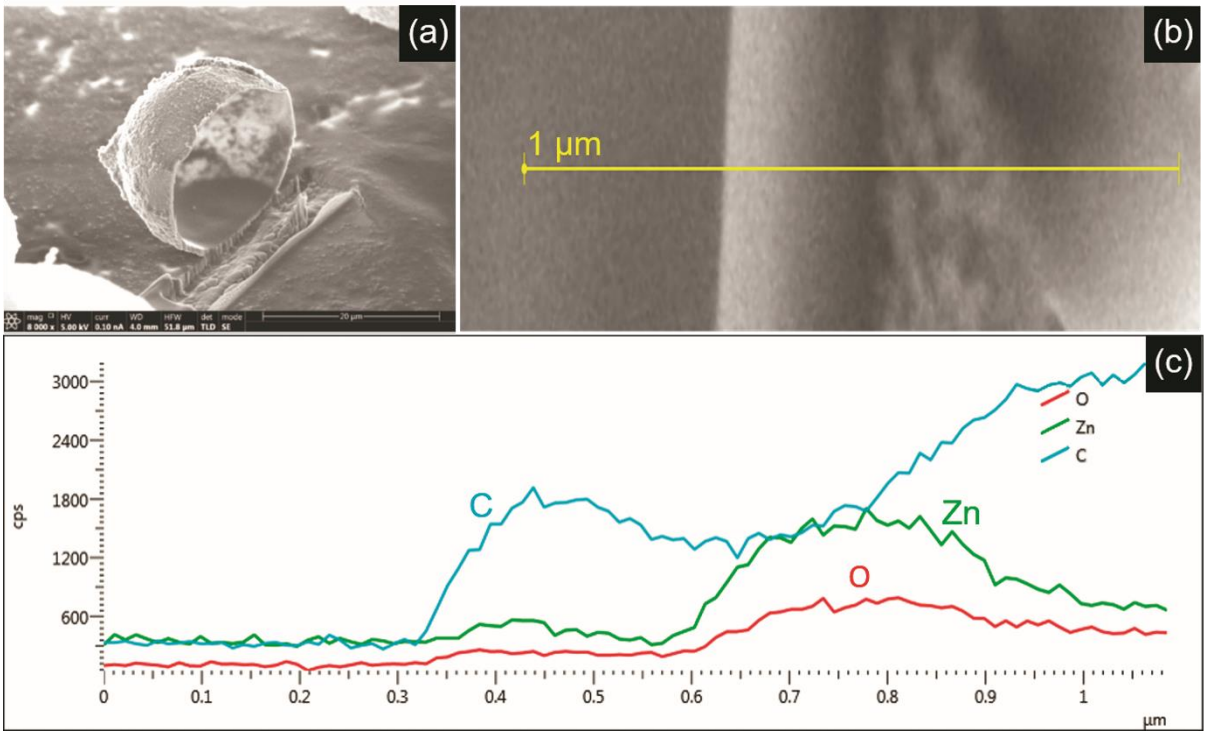

Figure 5. SEM images of cross-section of MCT28 microsphere supported by ZnO a), b) and a line scan of the microcapsule shell (c) showing that the zinc species coat the outer section of the carbonaceous shell of the PCM.

DSC analysis of the three zinc oxide coated materials was conducted at a scan rate of 5 °C min^{-1} over the range 5- 40 °C, and the energy under the exothermic and endothermic peaks were integrated giving latent heat of 129, 143 and 157 J g^{-1} for melting of MCT28-ZnO-1, MCT28-ZnO-2 and MCT28-ZnO-3, respectively. The heating and cooling latent heats differ by 5%, which is attributed to the change in the heat capacity, Cp vs temperature dependency.

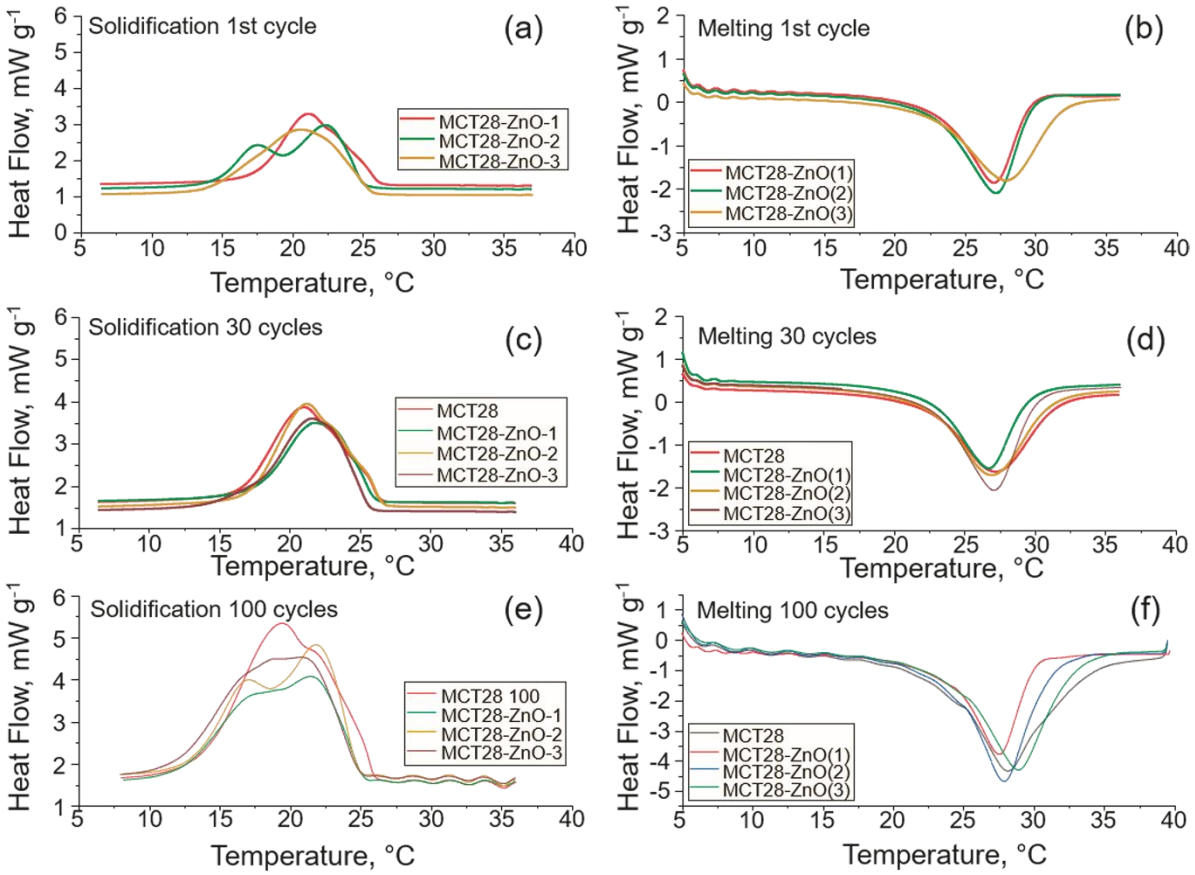

Figure 6. DSC data of zinc oxide coated microcapsules after 1st thermal cycling, 30th thermal cycling and 100th cycle.

The Cp of the melt is 17% higher compared to the Cp of the solid paraffin. In the integration of the heat of phase change, the sensible heat is approximated by straight lines between the melt and solid backgrounds. This is strictly accurate only when there is a constant rate of phase change. However, in reality, the melting and solidification rates depend on the temperature in a complex manner, and they are neither reversible nor linear. Therefore, the deviation of the Cp of the mixture of melt and solid from linearity is different for the endothermic and exothermic peaks. The relative percentage of the paraffin in the composite PCM can be approximated by the ratio between the observed heat of fusion and the heat of fusion of the paraffinic core alone. The latter was approximated as 256 J g^{-1} in our calculations. This ratio is depicted in column 7 of **Table 1**. The higher the zinc content the smaller the observed latent heat. We got also an independent estimate of the ZnO content by

thermogravimetry in air. The thermal weight loss curves of MCT28-ZnO-1, MCT-ZnO-2 and MCT28-ZnO-3 compared to MCT28 are depicted in **Figure 7**. In all cases, the thermograms follow an initial gradual weight loss up to 300 °C due evaporation of imbibed water and water formed by polycondensation of zinc hydroxide, a second steep decrease due to paraffin combustion, and a third phase due to the combustion of the melamine formaldehyde shell at 410-560 °C. Thus, the remaining zinc oxide is an underestimate of the initial zinc hydroxide shell and the imbibed reactants (mainly acetic acid, methanol and water). Indeed, the decrease of the paraffin core observed by the latent heat (5.7, 14 and 22.5%) is somewhat higher compared to the fraction of remaining zinc oxide (5, 9 and 12% for MCT28-ZnO-1, MCT28-ZnO-2 and MCT28-ZnO-3, respectively) after the high temperature combustion. We checked the stability of the DSC curve and the heat loss as a function of freeze/thaw cycling. **Figure 6** shows the DSC curves after 30 and 100 freeze-thaw cycles for the three ZnO coated PCMs. In all cases, the heat of fusion was approximately constant with less than 10% change between thirtieth and the hundredth cycles. Paraffins and organically encapsulated paraffins are hydrophobic and lighter than water and tend to separate from aqueous dispersion. An important benefit of the doubly coated PCMs is the ability to disperse them in aqueous solutions and other solvents. This is due to two attributes: first, zinc oxide has a higher specific density (5.6) compared to paraffin (specific gravity, 0.78 for n-octadecane), and thus it is possible to tailor the density of the beads by a small change in the inorganic content. In addition, the dispersibility of the inorganic, hydrophilic material is much better than that of the organic capsules. As a result, we received stable dispersions of MCT-ZnO-2 for the whole concentration range. **Figure 8** a-d shows the dispersibility of 10% bare MCT28, MCT28-ZnO-1, MCT28-ZnO-2 and MCT28-ZnO-3 in water. MCT28 and MCT-ZnO-3 slurries undergone phase separation and the PCM capsules immediately floated over the water, whereas the PCMs with the higher loadings formed stable dispersions and remained in a single phase even after several months without stirring.

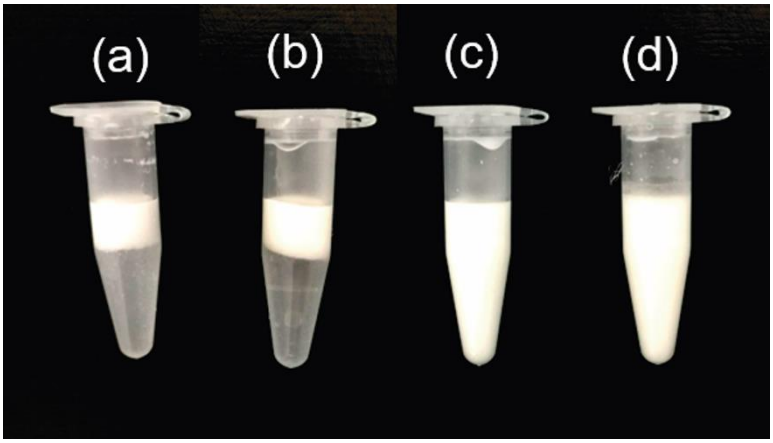

Figure 8. Dispersibility of 10% uncoated MCT28, MCT28-ZnO-3, MCT28-ZnO-2 and MCT28-ZnO-1 in water.

The observed thermal conductivity and thermal effusivity of the aqueous dispersion of the PCMs were improved compared to the uncoated PCMs due to the formation of the outer zinc oxide coating as can be shown in **Figure** 9. The main improvement is in the phase transition temperature range where the heat flow from the sensor to the sample is increased due to the phase change which forms local buffering of the temperature in the vicinity of the heat source. Since the PCM should operate near the phase transition temperature, this is the more significant range for heat storage materials. Faster heat flow at this range guarantees more complete phase transition and fuller utilization of the latent heat.

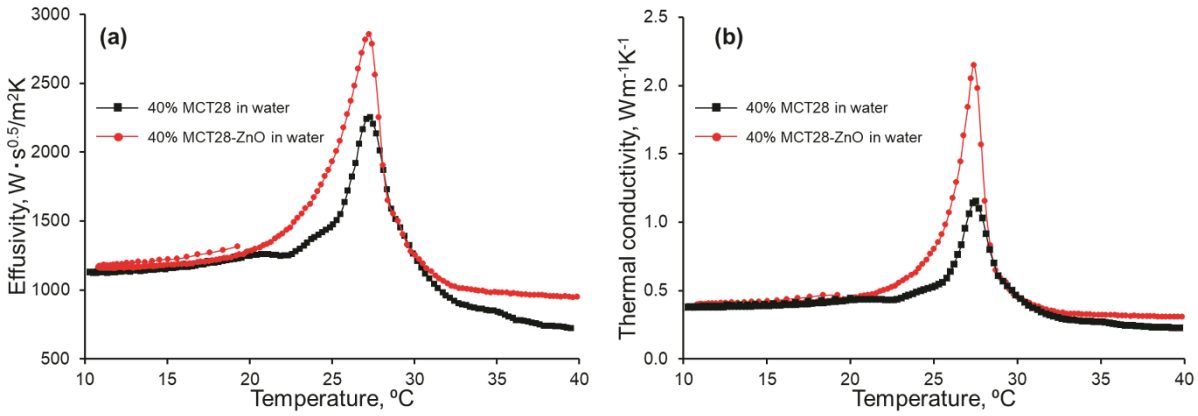

Figure 9. Thermal conductivity and effusivity of 40% wt. water dispersion of MCT28 and MCT28-ZnO-2.

3. Conclusion

We presented a way to benefit from the hermetic sealing provided by organic microencapsulation of PCMs as well as from the favorable attributes of inorganic microcapsules by uniform coating of the organic microcapsules by a thin zinc oxide layer. We showed that it is possible to obtain uniform coating of the organic microcapsules by zinc peroxide and to convert the zinc peroxide to zinc oxide by chemical treatment with sodium sulfite. Better dispersibility and improved thermal conductivity and effusivity were demonstrated. We anticipate that hydrogen peroxide sol-gel processing will allow formation of other post-transition element oxides as well and will increase the range of attainable PCM microcapsules and their compatibility to aqueous dispersion and hydrophilic substrates.

4. Experimental Section

ZnO coating of PCMs. 154 mg of zinc acetate dihydrate were dissolved in 2 mL of concentrated 28-30% NH_4OH solution. Then 5 mL of 10% hydrogen peroxide solution were added and subsequently 300 mg of MCT28 spheres (from Microtek Laboratories Inc.) were introduced under gentle stirring for 10 min. 15mL of 30 wt% hydrogen peroxide solution were added, slowly, drop by drop to the suspension with gentle stirring to obtain zinc peroxide precipitate on the PCM spheres. The product was separated by filtration on paper filter and washed 3 times by water and once by ethanol and then dried under vacuum for 30 min. Obtained powder was marked as MCT28-ZnO_2. Three different samples were synthesized with 154, 77 and 50 mg of zinc acetate dihydrate, denoted as MCT28-ZnO_2-1, MCT28-ZnO_2-2, and MCT28-ZnO_2-3, respectively. Then, to convert the zinc peroxide to zinc oxide, 1 gr of dry powder was dispersed in 40 ml of 0.1M Na_2SO_3 aqueous solution and left for 3 days with stirring with a magnetic stirrer under room temperature. The filtered and washed products are denoted MCT28-ZnO-1, MCT28-ZnO-2, and MCT28-ZnO-3. A similar procedure was used to prepare MCT68-ZnO beads.

Thermal conductivity measurements. Thermal conductivity measurement was performed using TCi Thermal Conductivity Analyzer (C-Therm Technologies Ltd, Canada) based on the modified transient plane source technique. The instrument allows determination of the effusivity and thermal conductivity of powders and homogeneous dispersions,[35,36] and therefore was chosen as the most useful thermal analyzer for this research. The value of thermal conductivity (k) was measured for powders and aqueous dispersion in the relevant temperature range, 10-40 °C for MCT28 or up to 80 °C for MCT68. The observed effusivity was measured by the same setup.

Differential scanning calorimetry (DSC) was performed on differential scanning calorimeter, DSC 822 Mettler, Toledo and *thermogravimetric analysis (TGA)* was conducted on Thermobalance, TG50 Mettler, Toledo. All experiments were carried out in the range 10-50 °C for MCT28 or 30-80 °C for MCT68 under nitrogen flow at a heating rate of 5 °C min^{-1}.

High Resolution Scanning Electron Microscope. SEM imaging was performed using the FEI Sirion High Resolution Scanning Electron Microscope (HR SEM, Eindhoven, Holland). Accelerating voltage was set at 5-15 kV with 5 mm working distance. Imaging was conducted using high resolution mode in an ultrasonic bath, and the suspension was then dropped on a silicon wafer to dry.

The Helios PFIB DualBeam. SEM imaging of cross section of particles was performed using the Helios PFIB DualBeam. Microscope (DB FIB, Hillsboro, USA). Accelerating voltage was set at 5-15 kV with 5 mm working distance. The specimen was prepared by placing of dried samples on a carbon tape.

X-ray powder diffraction. XRD measurements were performed on a D8 Advance Diffractometer (Bruker AXS, Karlsruhe, Germany). The powder samples were carefully filled into low background quartz sample holders. The specimen weight was approximately 0.5 g. XRD patterns from 5° to 75° 2θ were recorded at room temperature using CuKα radiation (k = 1.5418Å) under the following measurement conditions: tube voltage of 40 kV, tube current

of 40 mA, step scan mode with a step size 0.02° 2θ and counting time of 1 s/step. XRD patterns were processed using Diffrac Plus software.with a Through-the-Lens Detector.

Supporting Information

Supporting Information is available from the Wiley Online Library or from the author.

Acknowledgements

This research is partially supported by grants from the National Research Foundation, Prime Minister Office, Singapore under its Campus of Research Excellence and Technological Enterprise (CREATE) programme. The financial support of Israel Research Foundation and the Ministry of Science is thankfully acknowledged. We thank the Harvey M. Krueger Family Centre for Nanoscience and Nanotechnology of the Hebrew University of Jerusalem and the Israel Science Foundation. We thank the Russian Foundation for Basic Research (grant 18-29-19119). The publication was carried out within the State Assignment on Fundamental Research to the Kurnakov Institute of General and Inorganic Chemistry. This research was performed using equipment of the JRC PMR IGIC RAS.

Received: ((will be filled in by the editorial staff))
Revised: ((will be filled in by the editorial staff))
Published online: ((will be filled in by the editorial staff))

References

[1] M. M. Farid, A. M. Khudhair, S. A. K. Razack and S. Al-Hallaj, *Energy Convers. Manag.*, 2004, 45, 1597–1615.

[2] L. Liu, D. Su, Y. Tang and G. Fang, *Renew. Sustain. Energy Rev.*, 2016, **62**, 305–317.

[3] R. K. Sharma, P. Ganesan, V. V. Tyagi, H. S. C. Metselaar and S. C. Sandaran, *Energy Convers. Manag.*, 2015, **95**, 193–228.

[4] L. Liu, D. Su, Y. Tang and G. Fang, *Renew. Sustain. Energy Rev.*, 2016, **62**, 305–317.

[5] Z. Khan, Z. Khan and A. Ghafoor, *Energy Convers. Manag.*, 2016, 115, 132–158.

[6] Z. A. Qureshi, H. M. Ali and S. Khushnood, *Int. J. Heat Mass Transf.*, 2018, 127, 838–856.

[7] B. Li, T. Liu, L. Hu, Y. Wang and L. Gao, *ACS Sustain. Chem. Eng.*, 2013, **1**, 374–380.

[8] E. Onder, N. Sarier and E. Cimen, *Thermochim. Acta*, 2007, **467**, 63–72.

[9] Y. Jung, J. O. You and K. H. Youm, *Macromol. Res.*, 2015, **23**, 1004–1011.

[10] L. Cao, F. Tang and G. Fang, *Energy Build.*, 2014, **72**, 31–37.

[11] X. Ma, Y. Liu, H. Liu, L. Zhang, B. Xu and F. Xiao, *Sol. Energy Mater. Sol. Cells*, 2018, **188**, 73–80.

[12] J. F. Su, X. Y. Wang, S. B. Wang, Y. H. Zhao and Z. Huang, *Energy Convers. Manag.*, 2012, **55**, 101–107.

[13] K. Gopal Krishna Singlr, S. Haider, S. Patr and J. Wang, *Def. Sci. J.*, 2018, **68**, 218–224.

[14] N. Sarier, E. Onder and G. Ukuser, *Thermochim. Acta*, 2015, **613**, 17–27.

[15] K. Byrappa and Masahiro Yoshimura, *Handbook of hydrothermal technology A Technology for Crystal Growth and by*, Noyes Publications, 2001.

[16] Maggio P Pechini, US Pat. 304434A,1963.

[17] S. Sladkevich, N. Kyi, J. Gun, P. Prikhodchenko, S. Ischuk and O. Lev, *Thin Solid Films*, 2011, **520**, 152–158.

[18] M. F. Pereira, A. F. F. Farias, A. G. Souza, M. G. Fonseca, L. F. B. L. Pontes and I. M. G. Santos, *Cerâmica*, 2017, **63**, 82–89.

[19] S. Sladkevich, A. A. Mikhaylov, P. V. Prikhodchenko, T. A. Tripol'skaya and O. Lev, *Inorg. Chem.*, 2010, **49**, 9110–9112.

[20] Y. Wolanov, P. V. Prikhodchenko, A. G. Medvedev, R. Pedahzur and O. Lev, *Environ. Sci. Technol.*, 2013, **47**, 8769–8774.

[21] A. G. Medvedev, A. A. Mikhaylov, D. A. Grishanov, D. Y. W. Yu, J. Gun, S. Sladkevich, O. Lev and P. V. Prikhodchenko, *ACS Appl. Mater. Interfaces*, 2017, **9**, 9152–9160.

[22] A. A. Mikhaylov, A. G. Medvedev, C. W. Mason, A. Nagasubramanian, S. Madhavi, S. K. Batabyal, Q. Zhang, J. Gun, P. V. Prikhodchenko and O. Lev, *J. Mater. Chem. A*, 2015, **3**, 20681–20689.

[23] A. A. Mikhaylov, A. G. Medvedev, T. A. Tripol'skaya, V. S. Popov, A. S. Mokrushin, D. P. Krut'ko, P. V. Prikhodchenko and O. Lev, *Dalt. Trans.*, 2017, **46**, 16171–16179.

[24] X. X. Zhang, Y. F. Fan, X. M. Tao and K. L. Yick, *Mater. Chem. Phys.*, 2004, **88**, 300–307.

[25] X. X. Zhang, Y. F. Fan, X. M. Tao and K. L. Yick, *J. Colloid Interface Sci.*, 2005, **281**, 299–306.

[26] Microtek Laboratories, Inc., https://www.microteklabs.com.

[27] A. B. Djurišić, X. Chen, Y. H. Leung and A. Man Ching Ng, *J. Mater. Chem.*, 2012, **22**, 6526–6535.

[28] R. Jalal, E. K. Goharshadi, M. Abareshi, M. Moosavi, A. Yousefi and P. Nancarrow, *Mater. Chem. Phys.*, 2010, **121**, 198–201.

[29] EPA, 1991, 1–21.

[30] A. Yadav, V. Prasad, A. A. Kathe, S. Raj, D. Yadav, C. Sundaramoorthy and N. Vigneshwaran, in *Bulletin of Materials Science*, Springer India, 2006, vol. 29, pp. 641–645.

[31] F. Li, X. Wang and D. Wu, *Energy Convers. Manag.*, 2015, **106**, 873–885.

[32] P. V. Prikhodchenko, A. G. Medvedev, A. A. Mikhaylov, T. A. Tripol'Skaya, L. Cumbal, R. Shelkov, Y. Wolanov and J. Gun, *Mater. Lett.*, 2014, **116**, 282–285.

[33] I. Y. Chernyshov, M. V. Vener, P. V. Prikhodchenko, A. G. Medvedev, O. Lev and A. V. Churakov, *Cryst. Growth Des.*, 2017, **17**, 214–220.

[34] C. M. Wallen, J. Bacsa and C. C. Scarborough, *J. Am. Chem. Soc.*, 2015, **137**, 14606–14609.

[35] J. Cha, J. Seo and S. Kim, *J. Therm. Anal. Calorim.*, 2012, **109**, 295–300.

[36] S. Wi, S. G. Jeong, S. J. Chang, J. Lee and S. Kim, *Appl. Energy*, 2017, **205**, 1548–1559.

Possibility to obtain uniform coating of the organic microcapsules by zinc oxide were shown. Better dispersibility and improved thermal conductivity and effusivity were demonstrated. Hydrogen peroxide sol-gel processing will allow formation of other post-transition element oxides as well and will increase the range of attainable PCM microcapsules and their compatibility to aqueous dispersion and hydrophilic substrates.

Keyword Zinc Oxide coated PCM

A. A. Mikhaylov, A. G. Medvedev, D. A. Grishanov, S. Sladkevich, Z. J. Xu, K. A. Saharov, P. V. Prikhodchenko, O. Lev*

Doubly coated, organic – inorganic paraffin phase change materials: zinc oxide coating of hermetically encapsulated paraffins

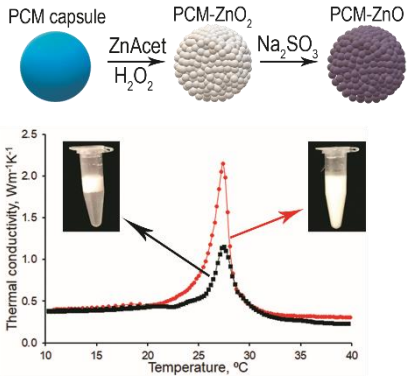

Supporting Information

Doubly coated, organic – inorganic paraffin phase change materials: zinc oxide coating of hermetically encapsulated paraffins

*Alexey A. Mikhaylov, Alexander G. Medvedev, Dmitry A. Grishanov, Sergey Sladkevich, Zhichuan J. Xu, Konstantin A. Saharov, Petr V. Prikhodchenko, Ovadia Lev**

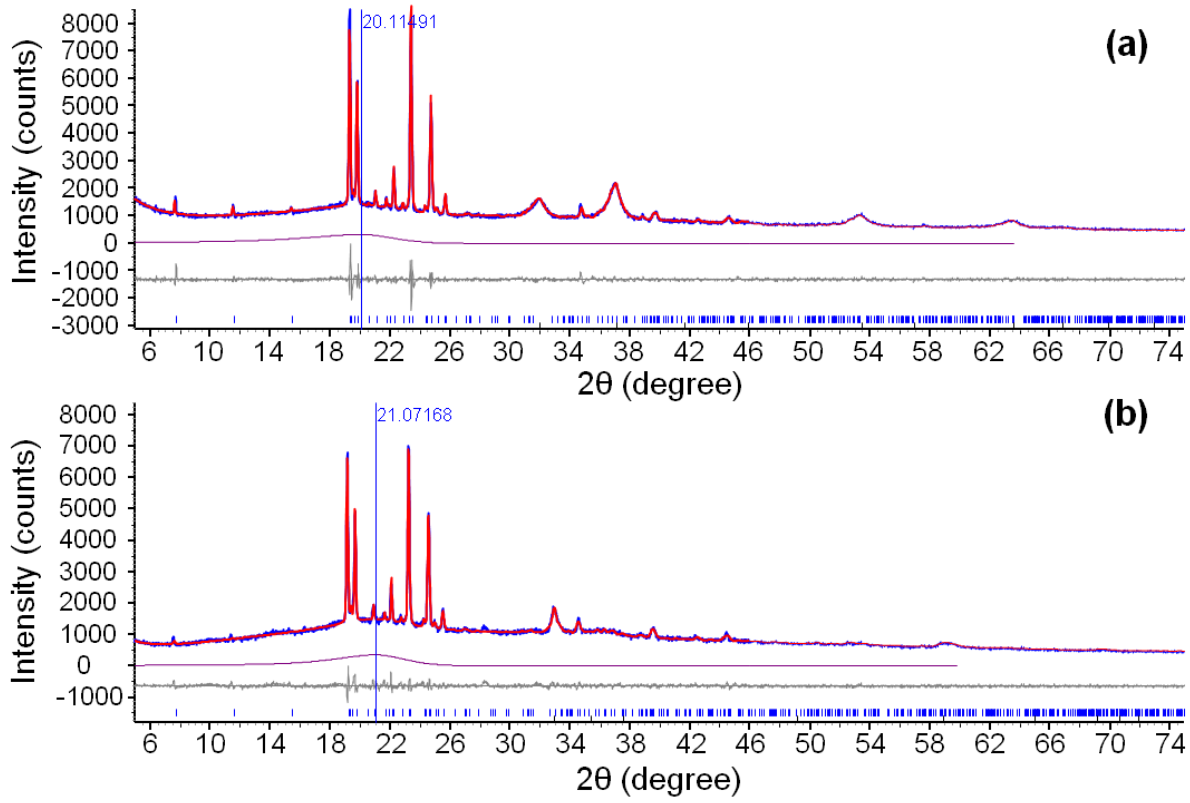

Figure S1**.** Rietveld refinement of powder XRD data of (a) MCT28-ZnO_2 and (b) MCT28-ZnO-2. Each frame presents (from top) the fitted (red line) and observed (blue line) spectra, the amorphous phase contribution, difference curve and positions of the Bragg diffractions of octadecane (blue bars) and ZnO_2 and ZnO (black bars) respectively.

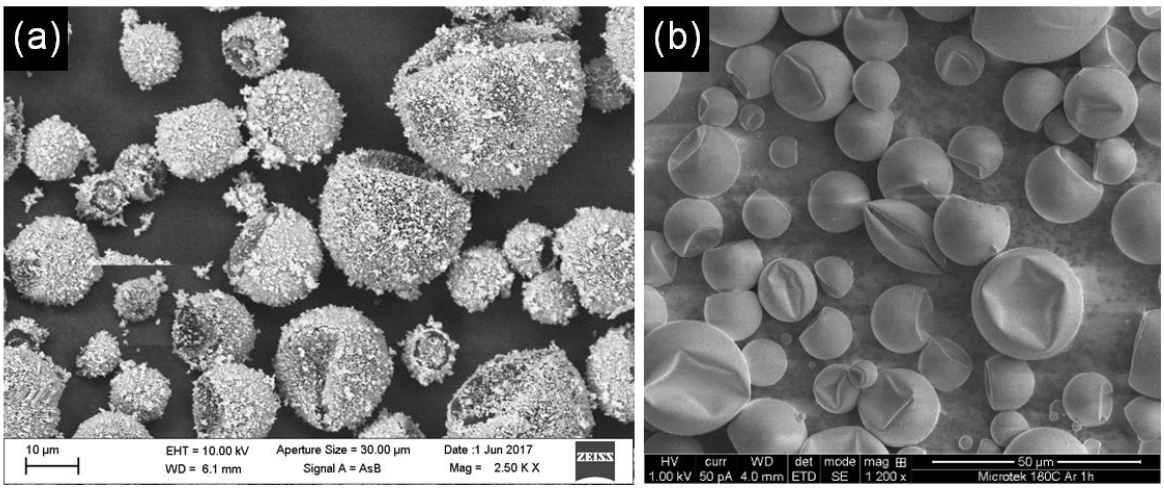

Figure S2. SEM image of distorted heat treated zinc dioxide coated MCT28 (a) and bare MCT28 (b) after heat treatment at 150 °C.

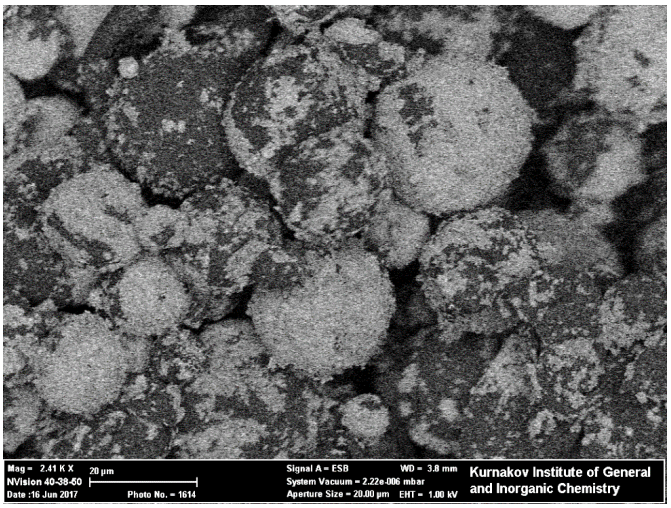

Figure S3. SEM image of partially peeled off zinc dioxide coated MCT28 after reduction by $NaBH_4$.

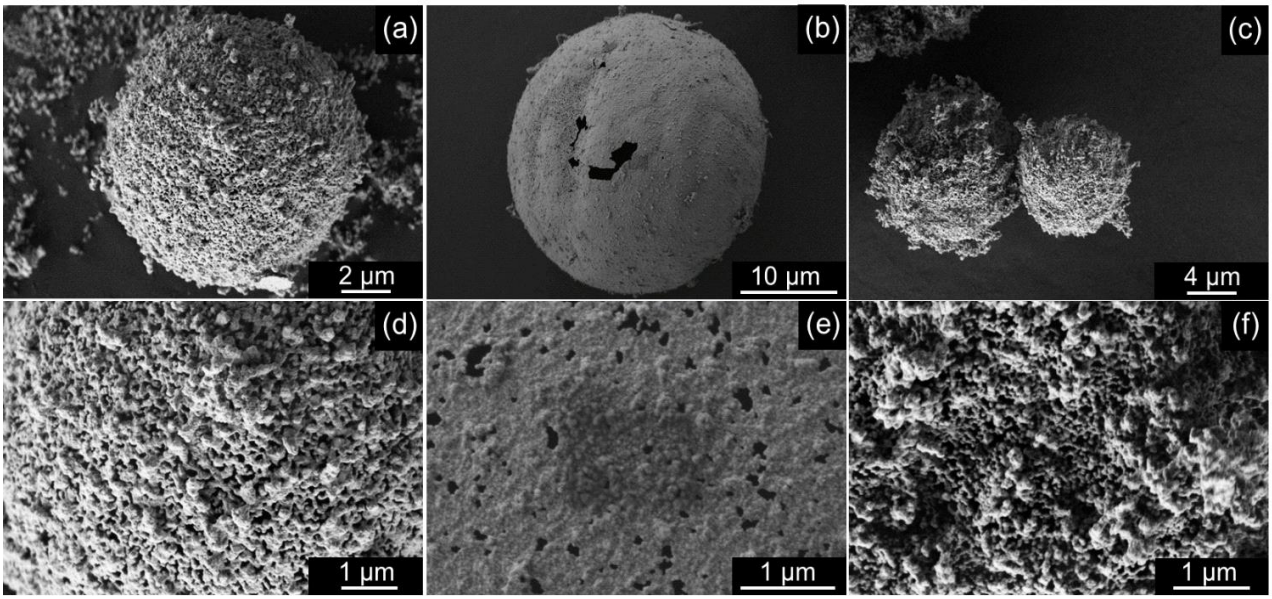

Figure S4. SEM images of MCT28-ZnO-1 (a, d)), MCT28-ZnO-2 (b, e)), MCT28-ZnO-(c, f)) at different magnifications after heat treatment at 900 °C in air.